

Supplementary information

***In Situ* Formed Uniform and Elastic SEI for High-Performance Batteries**

Mingyuan Gu¹, Apparao M. Rao², Jiang Zhou³, Bingan Lu^{1*}

¹School of Physics and Electronics, Hunan University, Changsha, P. R. China.

²Department of Physics and Astronomy, Clemson Nanomaterials Institute, Clemson University, Clemson, SC, USA.

³School of Materials Science and Engineering, Central South University, Changsha, 410083, P. R. China.

*Corresponding author. E-mail: luba2012@hnu.edu.cn (B. Lu)

Table of contents

1. Mechanism of ISEP and properties of different SEI	3
2. Properties of the electrolytes used in this work	5
3. Electrochemical performance of potassium metal symmetric batteries	10
4. Characterization of different SEI	17
5. Charge/discharge curves of Li Cu and Li graphite batteries with ISEP-SEI	21
6. Summary of the potassium metal symmetric battery information	22
7. References	23

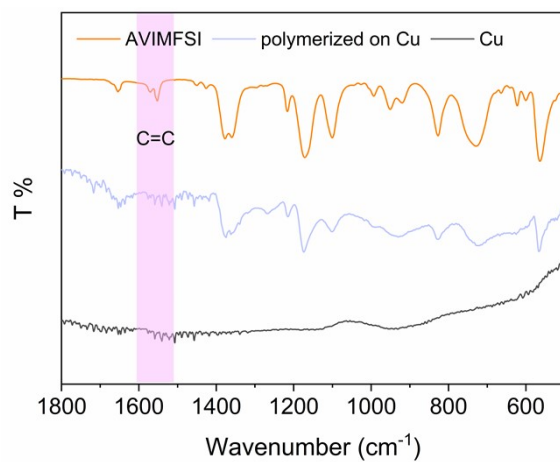


Fig. S1. Fourier transform infrared spectroscopy of AVIMFSI, blank Cu, and polymerized AVIMFSI on Cu.

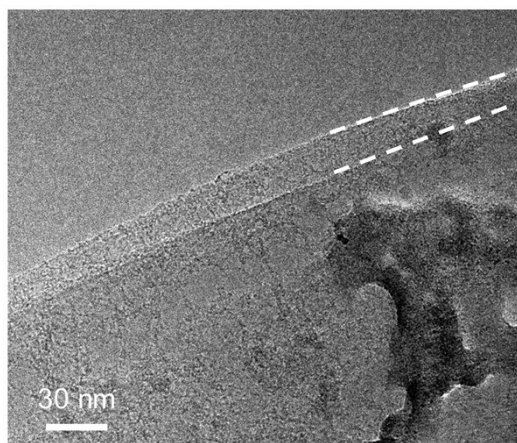


Fig. S2. TEM image of inorganic-rich SEI.

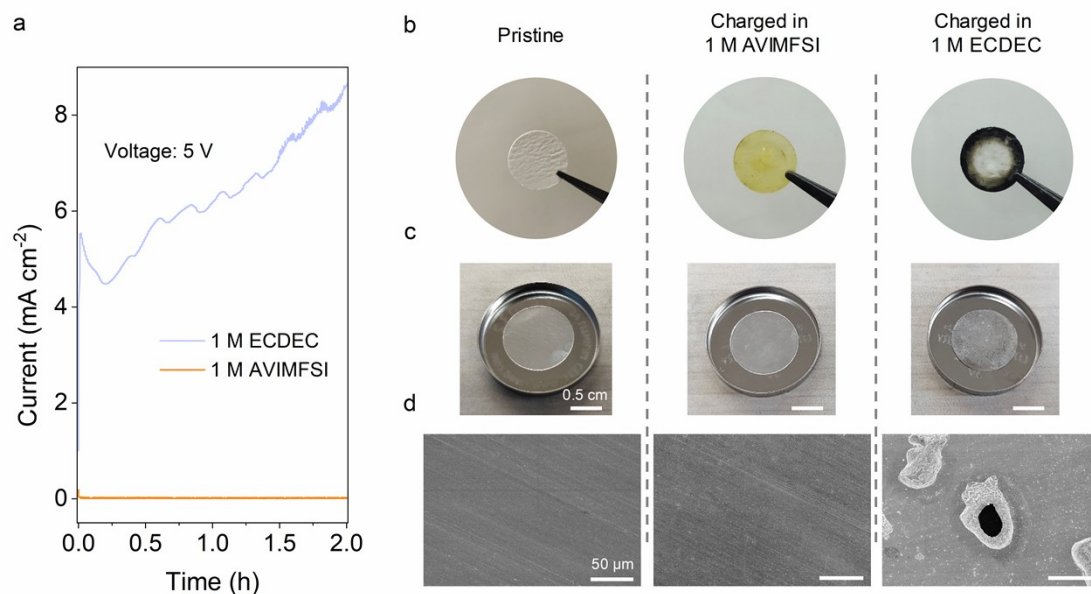


Fig. S3. Corroding properties of the two electrolytes on Al. **a**, Leakage current test under a constant voltage of 5 V for 2 h. **b**, Optical images of a pristine glass fiber separator and glass fiber separators charged in the two electrolytes. Optical and SEM images of pristine Al and Al charged in the two electrolytes (**c**, **d**).

Note 1: When charging for 2 h under a constant voltage of 5 V, the battery using 1 M AVIMFSI electrolyte showed almost no leakage current, indicating the negligible corrosion of Al¹. However, the battery with the 1 M ECDEC electrolyte showed a continuously increasing leakage current, indicating increasing corrosion of Al (**Supplementary Fig. S3a**). After disassembling the batteries, the optical images of the separators and the optical and SEM images of Al foils were obtained (**Supplementary Fig. S3b-d**). Compared with the pristine separator (**Supplementary Fig. S3b**), the one with 1 M AVIMFSI electrolyte showed almost no change, but the one with 1 M ECDEC electrolyte turned black, indicating the presence of undesired side reactions. The Al foil charged in 1 M AVIMFSI electrolyte was almost identical to the pristine Al foil (**Supplementary Figs. S3c and d**), implying negligible corrosion. However, the corrosiveness of 1 M ECDEC electrolyte resulted in the formation of many small pits in the Al foil, which was obvious in both optical and SEM images.

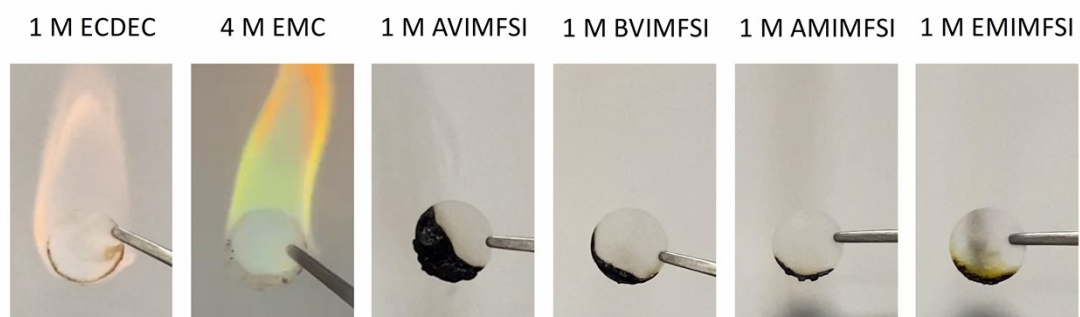


Fig. S4. Flame retardancy test of the six electrolytes used in this study.

Note 2: The 1 M ECDEC electrolyte and 4 M EMC electrolyte are both flammable. In contrast, the four ionic liquid electrolytes are all non-flammable.

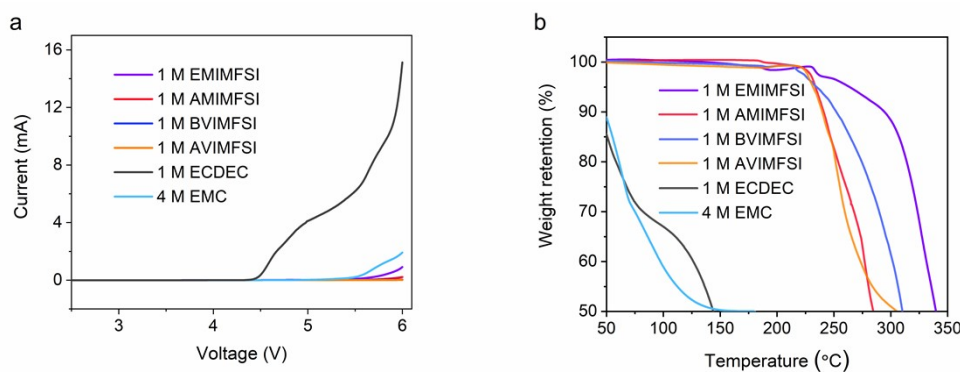


Fig. S5. Linear sweeping voltammetry (LSV) (a) and thermogravimetric analysis (TGA) results (b) of the six electrolytes.

Note 3: 1 M ECDEC electrolyte shows the lowest decomposition potential. After increasing the concentration of electrolyte (4 M EMC), the decomposition potential increases as well. The decomposition potential of the nonfunctional ionic liquid electrolyte is slightly higher than the concentrated one. The functional ionic liquid electrolytes have the highest decomposition potential (**Supplementary Fig. S5a**). For the four ionic liquid electrolytes, no significant weight loss was observed until 200 °C. In contrast, the 1 M ECDEC and 4 M EMC electrolytes showed a significant weight loss at the beginning and experienced continuous loss with the increasing temperature because of the volatile carbonate solvents (**Supplementary Fig. S5b**).

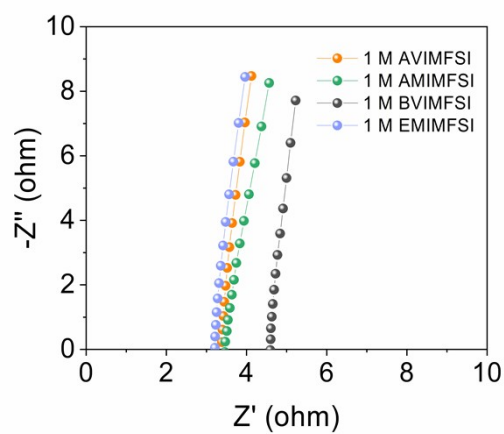
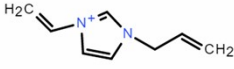
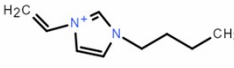
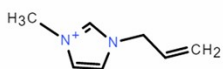
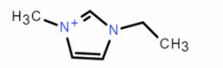


Fig. S6. Impedence spectra of the four ionic liquid electrolytes.

Cationic monomer	Abbreviation	Ionic conductivity (mS cm ⁻¹)	Decomposition temperature* (°C)
	AVIM ⁺	2.00	252
	BVIM ⁺	1.47	274
	AMIM ⁺	1.96	254
	EMIM ⁺	2.11	314

* The decomposition temperature refers to the temperature when the weight drops to 80%.

Fig. S7. Properties of the four ionic liquid electrolytes.

Note 4: The functional ionic liquid cationic monomers and their abbreviation are shown in **Supplementary Fig. S7**. The ionic conductivity of each ionic liquid electrolyte was calculated based on the test results shown in **Supplementary Fig. S6²**. The decomposition temperature was calculated based on the TGA results shown in **Supplementary Fig. S5b**.

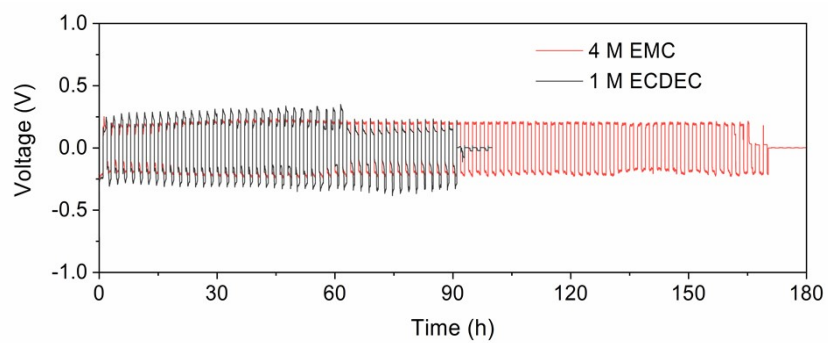


Fig. S8. Cycling performance of symmetric batteries with 1 M ECDEC and 4 M EMC electrolytes.

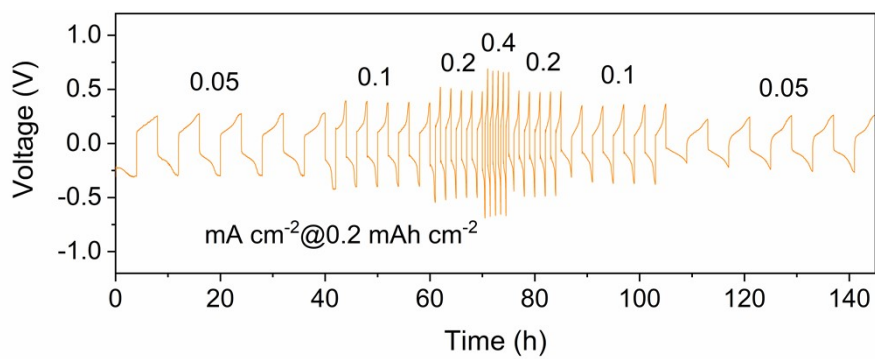


Fig. S9. Rate performance of symmetric batteries with 1 M AVIMFSI electrolyte.

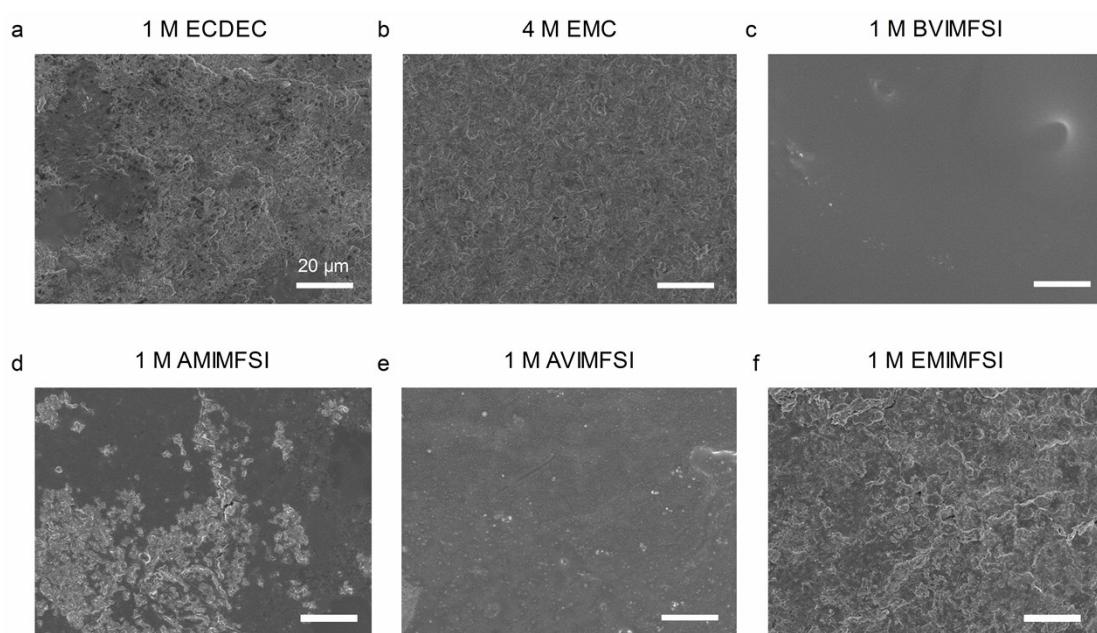


Fig. S10. Surface SEM images of potassium metal after cycling in the six electrolytes.

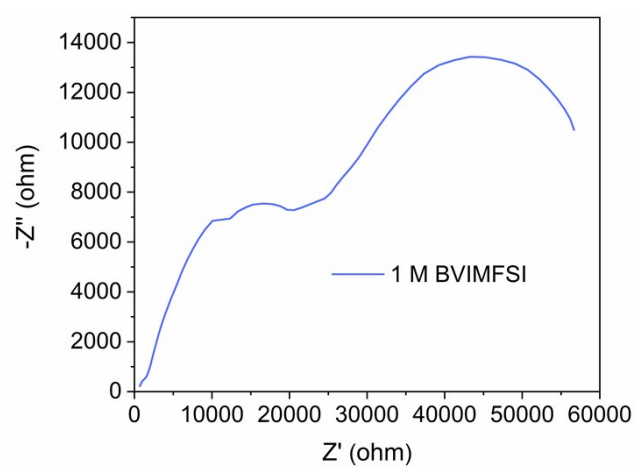


Fig. S11. EIS of symmetric batteries after cycling for 20 h with 1 M BVIMFSI electrolyte.

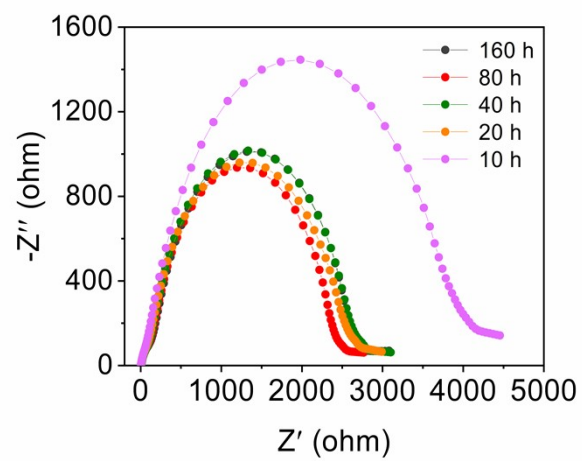


Fig. S12. EIS after different cycling times of symmetric batteries with 1 M AVIMFSI electrolyte.

1 M EMIMFSI

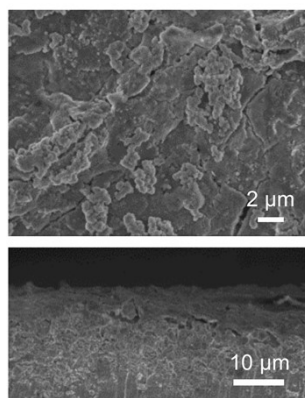


Fig. S13. SEM surface and cross-sectional images of potassium metal after cycling in 1 M EMIMFSI electrolyte.

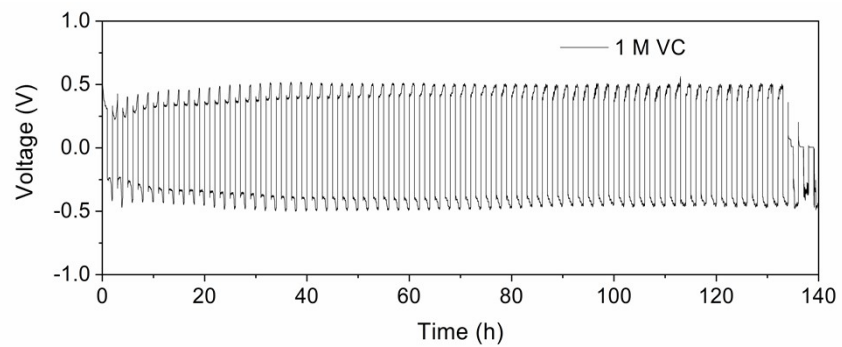


Fig. S14. Cycling performance of symmetric batteries with 1 M VC electrolyte.

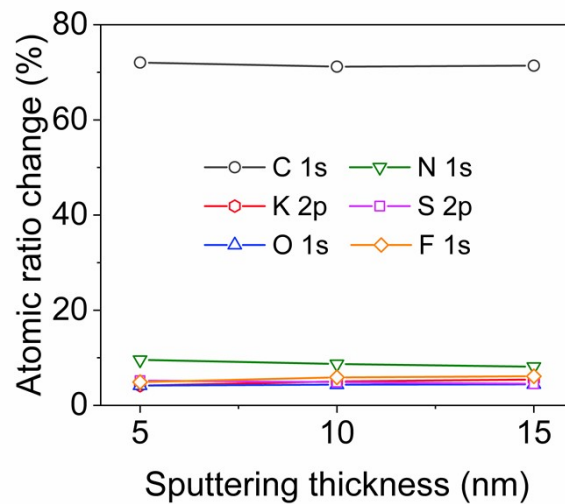


Fig. S15. Atomic ratio change of C 1s, N 1s, K 2p, S 2p, O 1s, and F 1s as a function of sputtered thickness.

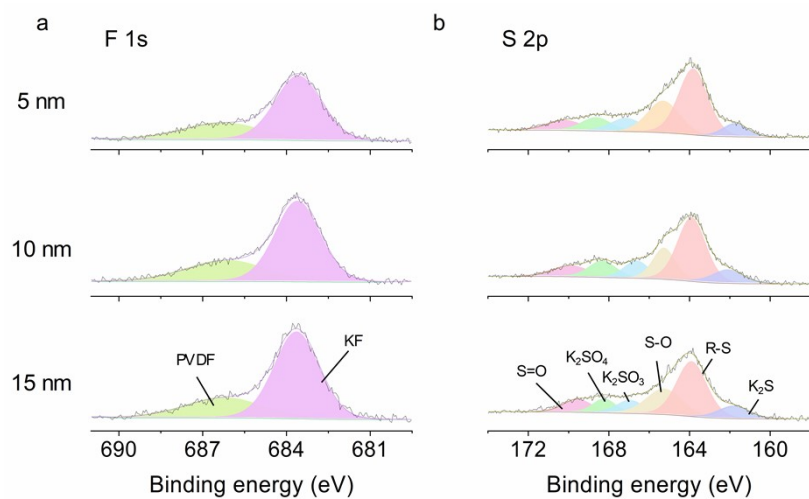


Fig. S16. XPS spectra of F 1s (a) and S 2p (b) collected from a graphite electrode sputtered to different thicknesses.

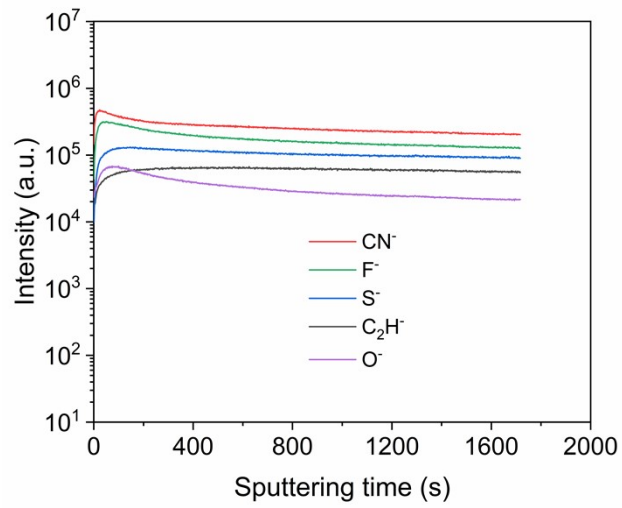


Fig. S17. Depth profiles of various secondary ions of interest contained in the sputtered area and volume.

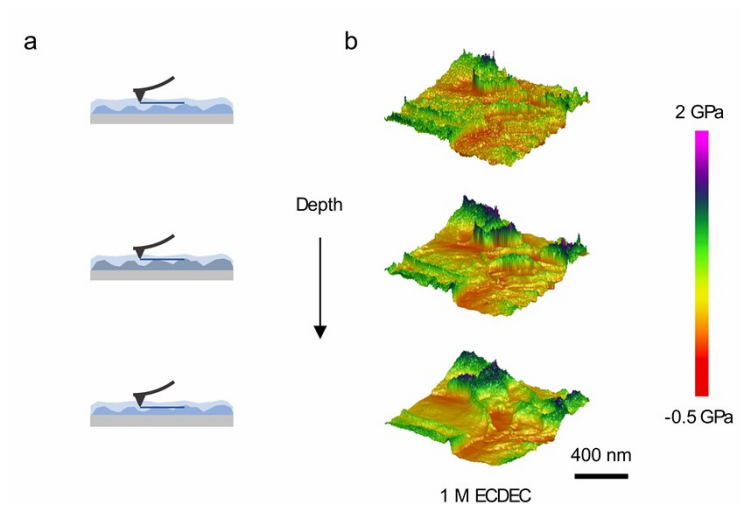


Fig. S18. **a**, Diagrams of DMT (elastic) modulus (E) test at different depths. **b**, DMT (elastic) modulus (E) mapping of organic-rich SEI formed in 1 M ECDEC electrolyte shown on a smaller modulus range (depth: ~8 nm, ~11 nm, ~15 nm).

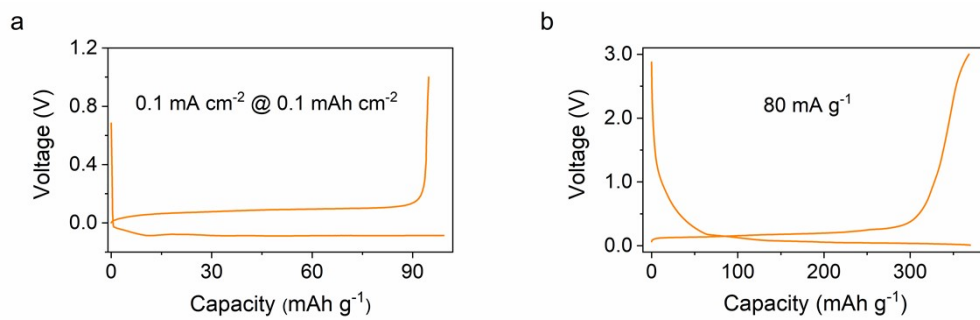


Fig. S19. **a**, Plating-stripping voltage curves of a Li||Cu battery. **b**, Charge-discharge voltage curves of a Li||graphite battery.

Table S1. The summary of the potassium metal symmetric battery information in different works.

Electrode	Electrolyte	Current density (mA cm ⁻²)	Area capacity (mAh cm ⁻²)	Cycling time (hour)
K metal ³	buffered K-Cl-IL	0.25	0.125	300
K metal ⁴	2.3 M KFSI in DME + 50 mM KNO ₃	0.05	0.15	300
Al@Al@K ⁵	4 M KFSI in DME	0.5	0.5	440
KxPy@K ⁶	1 M KTFSI in EC/DEC (1:1, w:w)	0.5	0.5	550
PVA- Borax@Cu@K ⁷	3 M KFSI in DME	0.5	0.25	700
K ₂ Te@K ⁸	1 M KFSI in EC/DEC (1:1, v:v)	0.5	0.5	800
CCPP ⁹	3 M KFSI in EC/DEC (1:1, v:v)	0.5	0.5	1000
Co-CNF@K ¹⁰	1 M KFSI in DME	0.5	0.5	1300
CBC@K ¹¹	1 M KFSI in DME	0.5	0.5	1400
PCNF@SnO ₂ @K ¹²	1 M KFSI in DME	0.5	0.5	1700
BVC@K ¹³	3 M KFSI in DME	0.1	0.2	1800
K metal ¹⁴	4 M KFSI in DME	0.5	0.5	2000
NC@GDY-Al ¹⁵	4 M KFSI in DME	0.2	0.2	2000
K metal (This work)	1 M KFSI in AVIMFSI	0.2	0.2	5000

References

1. S. Wei, S. Choudhury, J. Xu, P. Nath, Z. Tu and L. A. Archer, *Adv. Mater.*, 2017, **29**, 1605512.
2. C. Wang, A. C. Thenuwara, J. Luo, P. P. Shetty, M. T. McDowell, H. Zhu, S. Posada-Pérez, H. Xiong, G. Hautier and W. Li, *Nat. Commun.*, 2022, **13**, 4934.
3. H. Sun, P. Liang, G. Zhu, W. H. Hung, Y.-Y. Li, H.-C. Tai, C.-L. Huang, J. Li, Y. Meng, M. Angell, C.-A. Wang and H. Dai, *Proc. Natl. Acad. Sci.*, 2020, **117**, 27847-27853.
4. H. Wang, J. Dong, Q. Guo, W. Xu, H. Zhang, K. C. Lau, Y. Wei, J. Hu, D. Zhai and F. Kang, *Energy Storage Mater.*, 2021, **42**, 526-532.
5. P. Liu, Y. Wang, H. Hao, S. Basu, X. Feng, Y. Xu, J. A. Boscoboinik, J. Nanda, J. Watt and D. Mitlin, *Adv. Mater.*, 2020, **32**, 2002908.
6. P. Shi, S. Zhang, G. Lu, L. Wang, Y. Jiang, F. Liu, Y. Yao, H. Yang, M. Ma, S. Ye, X. Tao, Y. Feng, X. Wu, X. Rui and Y. Yu, *Adv. Energy Mater.*, 2021, **11**, 2003381.
7. S. Wang, Y. Yan, D. Xiong, G. Li, Y. Wang, F. Chen, S. Chen, B. Tian and Y. Shi, *Angew. Chem. Int. Ed.*, 2021, **60**, 25122-25127.
8. H. Yang, F. He, M. Li, F. Huang, Z. Chen, P. Shi, F. Liu, Y. Jiang, L. He, M. Gu and Y. Yu, *Adv. Mater.*, 2021, **33**, 2106353.
9. C. Qin, D. Wang, Y. Liu, P. Yang, T. Xie, L. Huang, H. Zou, G. Li and Y. Wu, *Nat. Commun.*, 2021, **12**, 7184.
10. L. Wang, H. Wang, M. Cheng, Y. Hong, M. Li, H. Su, J. Sun, J. Wang and Y. Xu, *ACS Appl. Energy Mater.*, 2021, **4**, 6245-6252.
11. M. Zhou, W. Qi, Z. Hu, M. Cheng, X. Zhao, P. Xiong, H. Su, M. Li, J. Hu and Y. Xu, *ACS Appl. Mater. Interfaces*, 2021, **13**, 17629-17638.
12. X. Zhao, F. Chen, J. Liu, M. Cheng, H. Su, J. Liu and Y. Xu, *J. Mater. Chem. A*, 2020, **8**, 5671-5678.
13. H. Ding, Y. Feng, J. Zhou, X. Yu, L. Fan and B. Lu, *Fundam. Res.*, 2022, DOI: 10.1016/j.fmre.2022.03.018.
14. P. Liu, H. Hao, H. Celio, J. Cui, M. Ren, Y. Wang, H. Dong, A. R. Chowdhury, T. Hutter, F. A. Perras, J. Nanda, J. Watt and D. Mitlin, *Adv. Mater.*, 2022, **34**, 2270058.
15. Y. Yi, J. Li, Z. Gao, W. Liu, Y. Zhao, M. Wang, W. Zhao, Y. Han, J. Sun and J. Zhang, *Adv. Mater.*, 2022, **34**, 2202685.